J Mater Sci (2007) 42:6887–6894
DOI 10.1007/s10853-007-1503-3

The influence of alloying $Fe_{59}Pt_{41}$ thin films with Co on their magnetic and microstructural properties

Yu Cheng Lai · Yen Hwei Chang · Yen Chia Chen · Hui-Jan Lin · Guo Jo Chen

Received: 8 February 2006 / Accepted: 5 January 2007 / Published online: 30 April 2007

Abstract This study investigates how the addition of Co to a $Fe_{59}Pt_{41}$ alloy with compositions in the range of $Fe_{59}Pt_{41}$–$Co_{59}Pt_{41}$ affects the crystallographic ordering temperatures and magnetic properties of sputter-deposited films. Introducing Co into the $(Fe_{1-x}Co_x)_{59}Pt_{41}$ film affects the activation energy of atomic migration and grain growth, thus leading to a higher annealing temperature of the $L1_0$ phase formation. At a Co concentration of $x = 0.2$, the saturation magnetization was maximum, at 1,480 emu/cm^3, and the $(Fe_{0.8}Co_{0.2})_{59}Pt_{41}$ film exhibited a coercivity of about 4 kOe.

Introduction

New media materials are required to increase the recording density of hard disk drives. Numerous studies of materials with a high uniaxial magnetic anisotropy constant (Ku) have been performed. Recent research has shown that the FeCo alloys have a maximum saturation magnetization (Ms) of 1,900 emu/cm^3 [1]. Burkert et al. [2] predicted from first principles that very specific structural distortions of FeCo alloys are associated with a high saturation magnetization that is approximately 50% larger than that of FePt.

For thin films of FePt and CoPt alloys, the crystal structure of the film deposited at room temperature is typically a face-centered cubic (fcc) disordered phase (a space group of Fm3 m), and these materials exhibit soft magnetic behavior. This fcc-FePt (CoPt) phase can be transformed to the hard magnetic face-centered-tetragonal (fct) $L1_0$-FePt (a space group of P4/mmm) ordered phase by annealing at high temperatures [3, 4]. The fcc-FePt or fcc-CoPt transforms to the $L1_0$-phase, which has its *c*-axis slightly smaller than its *a*-axis. The CoPt and FePt alloys have remarkable structures that are responsible for large magnetocrystalline anisotropy values of 2.8×10^6 and 7×10^6 J/m^3, respectively [5]. These values are very high so that the FePt and CoPt phases are expected to have very high coercivity as permanent magnets. The $L1_0$ ordered phase exhibits high magnetocrystalline anisotropy along the *c*-axis, which is caused by the strong hybridization of the d bands of Pt with the highly polarized d bands of Fe [6]. CoPt has a narrower fct phase field than FePt; Pt constitutes 35–63 at.% in FePt and around 37–53 at.% in CoPt at 700 °C [7].

The energy product quantity is given by presenting the largest rectangular area inscribed in the second quadrant of the B-H-diagram [8]. Studies of FePt permanent magnets in the form of thin films have yielded very interesting results, with an energy product as large as 318 kJ/m^3 obtained by intergranular exchange coupling [9]. The $L1_0$ equiatomically ordered FePt alloy is not one of the promising candidates as a medium material because of the extraordinary permanent magnetic characteristic specified by Hc = 100 kOe [10]. Increasing the anisotropy energy constant (Ku), however, also increases the media switching field, which is proportional to the ratio Ku/Ms, and cannot

Y. C. Lai (✉) · Y. H. Chang · Y. C. Chen · H.-J. Lin
Department of Material Science and Engineering, National Cheng Kung University, Tainan 70101, Taiwan, ROC
e-mail: enphei@mail.ncku.edu.tw

G. J. Chen
Department of Material Science and Engineering, I-Shou University, Kaohsiung County, Taiwan, ROC

exceed the write field capability of the head. The write field is believed to be near 5,000 Oe for longitudinal and possibly twice as large for perpendicular magnetic recording. [11]

The magnetic properties, crystallization and microstructures were examined in relation to the direction of magnetization. The Pt underlayer is critical to maintaining the *c*-axis of the crystal perpendicular to the film [12, 13]. Additionally, excellent crystallographic matching between the underlayer and the magnetic layer maintains a square loop, permitting narrow transition widths, governed by the direction of the easy axis. In addition, an underlayer has also been applied to promote the $L1_0$ phase transformation [14].

Few investigations of the magnetic properties of the polycrystalline materials $(Fe_{1-x}Co_x)_{59}Pt_{41}$ have been conducted. Recently, Chen et al. [15] have reported that $Fe_xCo_yPt_{100-x-y}$ alloy nanoparticles could be prepared by self-assembly. Based on their results, it was found that a phase transformation from disordered phase to $L1_0$ phase occurred during a 700 °C heat-treatment. They observed that the coercivity of alloy decreased with increasing cobalt content in the alloy.

The (FeCo)/Pt multilayer structures [16] exhibit perpendicular magnetic anisotropy. These thin films were fabricated on glass substrates by an electron beam evaporation. The [Pt(10 Å)/Fe(2.5 Å)/Pt(10 Å)] × *n* (*n* = 8–12) trilayers of films are sandwiched between Co layers of [Co(2.5 Å)/Pt(10 Å)] × *m* (*m* = 1–3). The anisotropy of Fe layers in (FeCo)/Pt multilayers may be induced by the interlayer interaction between the Fe and Co layers via polarization of Pt. In addition, (FeCo)Pt bulk alloys were prepared by induction melting, mechanical milling, hot and cold work, and melt extraction. Preliminary examination of the structural and magnetic properties of these alloys indicates that the (FeCo)Pt bulk alloys are an excellent system for exploring the exchange coupling mechanism in permanent magnets [17].

Most experimental studies [18] have used $Fe_{50}Pt_{50}$. Watanabe and Masumoto [19] reported remarkable permanent magnetic features of an $L1_0$-FePt bulk material, which was composed of a greater atomic ratio of Fe rather than equal stoichiometric $Fe_{50}Pt_{50}$. If the magnetic Fe layer is replaced by a $Fe_{1-x}Co_x$ alloy [2], the Co concentration (x) tailors the saturation magnetization within a wide range. In addition, Co is the only one of the three common room temperature ferromagnetic elements to have uniaxial symmetry, and hence be ideal for digital recording. [20]. Furthermore, Co has a higher resistance to chemical corrosion [21]. The above facts suggest that $(Fe_{1-x}Co_x)_{59}Pt_{41}$ may have the magnetic characteristics (high saturization magnetization) of FeCo and the coercivity of the FePt.

This work attempts to alter the magnetic characteristic by using $Fe_{59}Pt_{41}$ rather than $Fe_{50}Pt_{50}$ and various concentrations of cobalt to prepare the $(Fe_{1-x}Co_x)_{59}Pt_{41}$ magnetic films on a Pt underlayer. The changes in the crystal structure, microstructure, and the magnetic characteristics of these alloy films are also investigated.

Experiment

The thin film system in this study consists of a magnetic layer and a Pt underlayer grown on the Si substrate. Before the 200 nm-thick Pt underlayer could be deposited, a Ti adhesive layer and a SiO_2 layer had to be deposited on the Si substrate because of the lattice mismatch. The approximately 5 cm (2 inch) diameter target of $Fe_{1-x}Co_x$ (x = 0, 0.2, 0.4, 0.6, 0.8, 1.0) alloys were prepared by rf melting in order to sputter deposit the $(Fe_{1-x}Co_x)_{59}Pt_{41}$ alloy films. The purity of the cobalt was 99.99% and that of the iron was 99.97%. The Pt pieces were pasted on the cast FeCo alloys to form FeCoPt composite targets. DC magnetron sputtering deposition was performed in an atmosphere of ultra clean argon gas at a pressure of 6.666 Pa, and the base pressure of the system was less than 1.333×10^{-4} Pa. The growth rate of the $(Fe_{1-x}Co_x)_{59}Pt_{41}$ thin films was controlled at 2.5 nm s^{-1}, and the normal thickness was evaluated based on the sputtering time and the microstructural evaluation of cross-section specimens of the films. The thickness of the magnetic alloy films was about 80 nm. The composition of the targets was measured by using inductively coupled plasma mass spectrometry (ICP-MS). The sputtering yield [22] of Fe, Co and Pt is Ys_{Fe} = 1.8 atoms/Ar^+, Ys_{Co} = 1.7 atoms/Ar^+ and Ys_{Pt} = 1.6 atoms/Ar^+, respectively. The morphology of the thin film was observed by a field emission scanning electron microscope (FESEM, Philips XL-40FEG) at an operating voltage of 15 kV without a conductive thin layer coating. The composition of alloy films was measured by using energy dispersive X-ray spectroscopy (EDX) which revealed the composition of alloy films was close to the targets. The substrate temperature was fixed at T_s = 500 °C and subsequent annealing was performed at 500 °C; the substrate was then held at 600 °C for 1 h in a vacuum. The vacuum level of the vacuum heat treatment was less than 6×10^{-5} Pa. X-ray diffraction was conducted before and after the heat treatment to detect structural changes. The crystal structures of the samples were characterized by multipurpose X-ray thin film diffractometry (XRD, Rigaku RINT 200). The ordering parameter, S, of these samples was evaluated using the integrated intensities of the (001) and (111) peaks extracted from fits to scans over these peaks [23]. The intensities of the observed peaks were obtained by calculating the integrated area of the characteristic peak of the X-ray

diffraction. The ordering parameter S was defined as the probability of correct site occupation in the $L1_0$ lattice, and is given by Eq. 1,

$$S^2 = \left(\frac{I(hkl)_{\text{sup.}}}{I(hkl)_{\text{fund.}}}\right) \times \left(\frac{4 \cdot L(\theta)_{\text{fund.}} \cdot P(\theta)_{\text{fund.}} \cdot e^{-2M(\theta)_{\text{fund.}}}}{L(\theta)_{\text{sup.}} \cdot P(\theta)_{\text{sup.}} \cdot e^{-2M(\theta)_{\text{sup.}}}}\right) \times \left(\frac{X_{\text{Fe}} \cdot f(\theta)_{\text{Fe}} + X_{\text{Pt}} \cdot f(\theta)_{\text{Pt}}}{f(\theta)_{\text{Fe}} - f(\theta)_{\text{Pt}}}\right)^2 = \frac{\left(\frac{I(001)_{\text{sup.}}}{I(111)_{\text{fund.}}}\right)_{\text{measure}}}{\left(\frac{I(001)_{\text{sup.}}}{I(111)_{\text{fund.}}}\right)_{\text{calculate}}}$$

$I(hkl) = C_o F(hkl)^2 LPA e^{-2M}$; $I(hkl)$ is the integrated intensity of the (hkl) diffraction peak; C_0 is a constant which depends on the incident intensity. $F = 4(x_{\text{Fe}} f_{\text{Fe}} + x_{\text{Pt}} f_{\text{Pt}})$ and $F = 2S(f_{\text{Fe}} - f_{\text{Pt}})$ are the structure factors for fundamental peaks and superlattice peaks respectively. $f(\theta)$ and $e^{-2M(\theta)}$ indicate the atomic scattering factor and Debye-Waller corrections respectively. I_{001} and I_{111} are the integrated intensities of (001) superlattice and (111) fundamental diffractions, respectively, and $(I_{001}/I_{111})_{\text{meas}}$ and $(I_{001}/I_{111})_{\text{cal}}$ are the measured and calculated diffraction intensity ratios, respectively. The structure factor of the superlattice peaks is proportional to S; hence the superlattice intensity is proportional to S^2, with the proportionality constant dependent on the chemically ordered phase and whether the film is epitaxial or polycrystalline. $(I_{001}/I_{111})_{\text{cal}}$ is related to the absorption factor, the Lorentz-polarization factor and structural factors [24, 25].

The microstructures of the thin films were characterized using a 200 kV high resolution transmission electron microscope (HRTEM, Philips Tecnai G2 F20 FEG-TEM). A superconducting quantum interference device magnetometer (SQUID, MPMS XL) was utilized to plot the hysteresis loops in magnetic fields of up to 5 Tesla.

Results and discussion

The crystal structures of the $(Fe_{1-x}Co_x)_{59}Pt_{41}$ films with various Co concentrations were determined by XRD. The XRD spectra of as-deposited films in the range of Co contents $0 \leq x \leq 1$ at $T_s = 500$ °C revealed the presence of fcc, fct and the mixed fct and fcc structures. The alloy films ($x = 0$ and $x = 0.2$) that contained a high iron concentration exhibited the $L1_0$ ordered phase. Alloys that contain Co from $x = 0.4$ to $x = 1$ tended to exhibit predominantly disordered fcc structure (JCPDS 29-0717), suggesting that during deposition the $(Fe_{1-x}Co_x)_{59}Pt_{41}$ films with a high iron concentration are transformed from disordered fcc to $L1_0$ phase at $T_s = 500$ °C, since FePt alloys have a lower transformation activation energy than CoPt [26]. Ostanin et al. [3] reported that the crystal structure of a FePt film, deposited at room temperature, is typically a fcc-FePt disordered phase when it is thermodynamically metastable [4]. This fcc phase can be transformed to fct $L1_0$ ordered phase by annealing at high temperature, since the ordered phase is thermodynamically stable at room temperature. Thermal annealing or the use of a heated substrate supplies energy to overcome the energy barrier of the ordering transition. For this reason, the as-deposited films that had a high Co concentration were annealed at various temperatures, as shown in Fig. 1. The crystal structure of the $(Fe_{0.2}Co_{0.8})_{59}Pt_{41}$ alloy film begins to change when it is annealed at 500 °C for 1 h. The (001) and (110) diffraction peaks were compared with those of the as-deposited film at $T_s = 500$ °C. Heat treatment at $T_a = 600$ °C yielded $(Fe_{0.2}Co_{0.8})_{59}Pt_{41}$ (001) and (110) superlattice reflections, and (200) and (002) fundamental reflections were also identified. Interestingly, the original fcc (200) peak splits into fct (200) and fct (002) peaks, which indicates that the phase transition to the ordered phase has to be induced at a relatively higher temperature for high Co content films. The XRD spectrum of $Co_{59}Pt_{41}$ included broad diffraction peaks, and the peak intensity $I_{\text{fct}(002)}$ was too weak to be identified, as shown in Fig. 2. The $Co_{59}Pt_{41}$ film yields a shoulder at around $2\theta = 47°$, revealing that the $L1_0$ phase of $Co_{59}Pt_{41}$ initially grew through nucleation and grain growth as the ordered fct phase from the fcc parent phase.

Heat treatment at 600 °C for 1 h showed that all alloy films were the ordered fct phase, except for $Co_{59}Pt_{41}$. The temperature required for the formation of the $L1_0$ phase

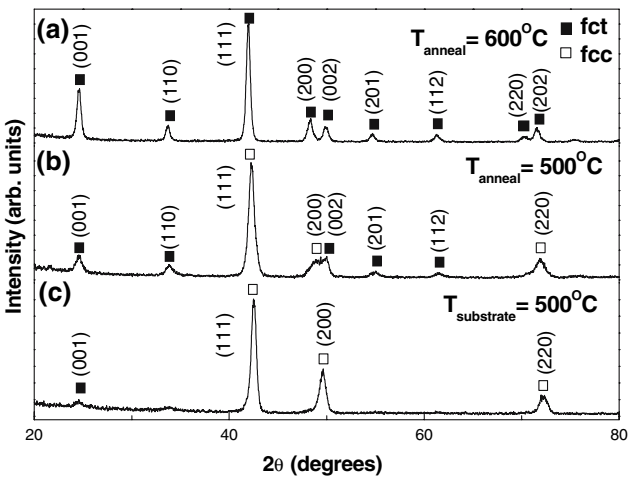

Fig. 1 X-ray diffraction patterns of $(Fe_{0.2}Co_{0.8})_{59}Pt_{41}$ film annealed at different temperatures for 1 h; the crystal structure of alloy film is (**a**) complete fct phase for $T_{\text{anneal}} = 600$ °C; (**b**) partial fcc + fct phases for $T_{\text{anneal}} = 500$ °C; (**c**) predominant fcc + fct phases for $T_s = 500$ °C

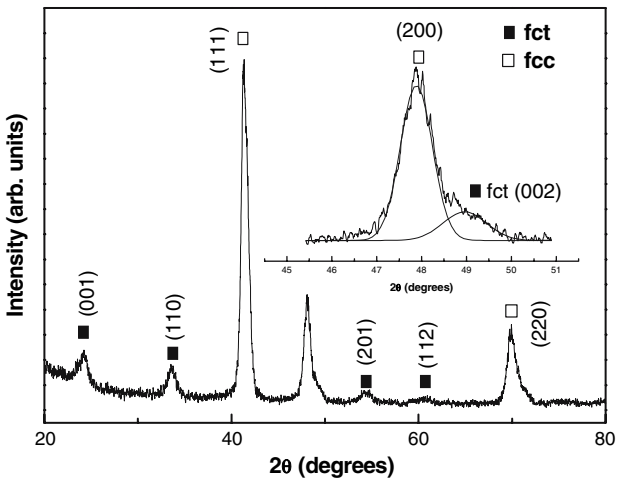

Fig. 2 X-ray diffraction patterns of $Co_{59}Pt_{41}$ film annealed at T_{anneal} = 600 °C for 1 h

increased according to the number of Co atoms replacing Fe atoms.

According to phase diagram [27], the larger magnitude of the transformation enthalpy together with the higher equilibrium ordering temperature for FePt (1,300 °C) when compared to CoPt (740 °C) result in a higher driving force, and thus a lower nucleation barrier for $L1_0$ formation in the former. Therefore, FePt should transform at lower temperatures than CoPt. However, the rates of transformation depend on the atomic mobility.

The superlattice diffraction line is characteristic of the ordered $L1_0$ phase. The superlattice reflections resulting from the $L1_0$ ordered phase are observed in the XRD diffraction pattern (Fig. 1). The fundamental diffraction lines in the ordered $L1_0$ phase are (111), (200) and (002), and the superlattice diffraction lines are (001), (110) and (201). For films annealed at T_a = 600 °C, the (001) and (110) superlattice reflection becomes weaker as the Co content increases, because the Fe atoms and Pt atoms that exhibit long range order were disturbed by Co atoms. The XRD pattern of the $L1_0$ samples demonstrates that the (111) peak shifted toward a higher angle because the formation of the $L1_0$ phase reduced the d-spacing of the (111) plane [28]. Not only do the Co atoms occupy the Fe sites in the FePt crystal (radius of Fe = 0.126 and radius of Co = 0.125 nm), but also the (111) peaks are shifted slightly toward a higher angle. As stated above, introducing Co into the $(Fe_{1-x}Co_x)_{59}Pt_{41}$ system reduced the d-spacing of the (111) plane but did not promote the formation of the $L1_0$ phase. The temperature required for the formation of the $L1_0$ phase increased according to the number of Co atoms replacing Fe atoms. $Co_{59}Pt_{41}$ was only completely transformed following annealing at T_a = 700 °C for 4 h. The annealing time and temperature required for the formation of the $L1_0$ phase increased when all of the Fe atoms were replaced with Co atoms. Figure 3 plots the dependence of the c/a ratio and that of the ordering parameter S on the Co content (x) in the $(Fe_{1-x}Co_x)_{59}Pt_{41}$ alloy, to understand how the degree of ordering varies with the addition of Co. The results showed that a variation in the ordering parameters from S_{FePt} = 0.79 to S_{CoPt} = 0.41 with increasing Co content is compatible with the change in c/a ratio from $c/a_{FePt} = 0.96112 \pm 4.149 \times 10^{-4}$ to $c/a_{CoPt} = 0.97631 \pm 8.846 \times 10^{-4}$.

The c/a ratio of the $(Fe_{1-x}Co_x)_{59}Pt_{41}$ films increased with increasing Co content. Accordingly, a smaller c/a ratio corresponds to a higher degree of ordering. Compared with c/a_{CoPt} = 0.97510 of the ordered $Co_{59}Pt_{41}$ phase (T_a = 700 °C for 4 h), the c/a_{CoPt} = 0.97631 annealing for 1 h was larger, and the degree of ordering declined markedly because the $Co_{59}Pt_{41}$ film had a greater fcc phase volume and a smaller $L1_0$ phase volume, indicating that $Co_{59}Pt_{41}$ exhibited a higher nucleation barrier to the formation of the $L1_0$ phase.

Figure 4 depicts the surface morphologies of the $(Fe_{1-x}Co_x)_{59}Pt_{41}$ films with different Co contents (x = 0, 0.2, 0.4, 0.6, 0.8, 1.0). Without Co, the particle size of the as-deposited $Fe_{59}Pt_{41}$ films is approximately 20 nm, and the distribution of particle sizes is highly uniform. In the $(Fe_{0.8}Co_{0.2})_{59}Pt_{41}$ films, the particles are approximately 30 nm, and are coarser than those in the $Fe_{59}Pt_{41}$ films. Some particles are clustered and the surface morphology is changed. When Co is alloyed at x = 0.4, the grain configuration was comparatively unclear. As the Co content was increased, the morphologies of the $(Fe_{0.4}Co_{0.6})_{59}Pt_{41}$ and $(Fe_{0.2}Co_{0.8})_{59}Pt_{41}$ film became more indefinite/irregular. At T_s = 500 °C, the surface morphology of ternary alloy films changed due to alloying with the third element, Co. Additionally, the configuration of the grains in $Co_{59}Pt_{41}$ films is evident, and the sizes of the grains appeared to be less homogenously distributed than those in the $Fe_{59}Pt_{41}$ film.

With the exception of the $Fe_{59}Pt_{41}$ and $Co_{59}Pt_{41}$ films, increasing the Co concentration resulted in a change in the surface morphology, which may imply that the Co concentration affects the activation energy of the migration of atoms and grain growth in ternary alloy films during the transformation of the $L1_0$ phase. Toney et al. [29] proposed that the FePt grain size of the fcc phase or untransformed phase is much smaller than that of the $L1_0$ phase. This is due to the formation of the $L1_0$ phase by nucleation and growth; once this phase forms, it grows quickly (since it is thermodynamically stable), whereas the untransformed fcc part of the film does not grow significantly. As shown in the XRD patterns (Fig. 1), the as-deposited films containing Co exhibit less $L1_0$ phase and retain more disordered fcc phase, indicating nucleation of the ordered phase from

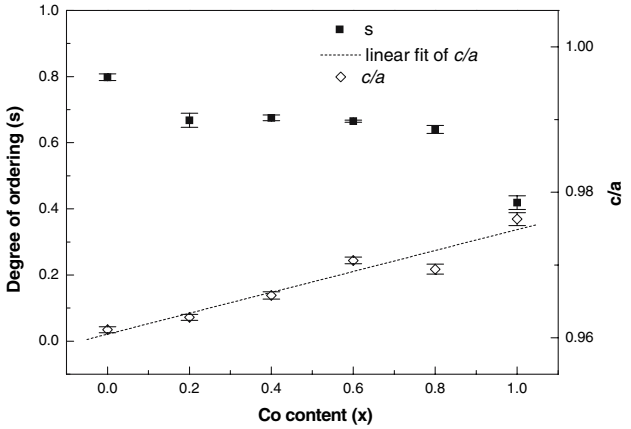

Fig. 3 Dependence of the *c/a* ratio of $(Fe_{1-x}Co_x)_{59}Pt_{41}$ and the variations of degree of ordering (S) on Co content after annealing at 600 °C for 1 h

the disordered matrix. This means that the ternary alloy as-deposited films tend to exhibit coexistence of ordered/disordered phases. According to Toney et al. [29], the grain size of the fcc phase is much smaller than that of the $L1_0$ phase. Therefore grain size distribution in the ternary alloy as-deposited film is broadened. For this reason, the surface morphology changed with the Co additive in the $(Fe_{1-x}Co_x)_{59}Pt_{41}$ films.

Figure 5 shows a bright-field TEM image of the $(Fe_{0.8}Co_{0.2})_{59}Pt_{41}$ alloy film. The selected area electron diffraction pattern revealed that the alloy film contained numerous grains with variously orientated *c*-axes, as shown in Fig. 5. In polycrystalline alloy films, the grains were not generally orientated perpendicularly to the film plane (substrate), because the use of lattice parameters to control the grain epitaxy reaches a maximum distance for film thicknesses of less than 40 nm [30]. Figure 6 presents a high-resolution TEM cross-sectional image of an $(Fe_{0.8}Co_{0.2})_{59}Pt_{41}$ film and the corresponding selected area diffraction (SAD) pattern. Interestingly, the image displays at least two kinds of defects in a single grain, including dislocations and twins. The inset shows the SAD pattern in the twin plane; the SAD pattern shows the twin reflections according to the twin plane {111}. The index of (200)t means that it is a symmetric twin spot (200). In Fig. 6, polytwin crystallites with a width of 60 nm are evident. The polytwin present in the $L1_0$ phase has twin planes that are parallel to {111}. The {111} twins in the $L1_0$-phase FePt films have also been reported in other work [31]. Polytwin structures are formed because of the nucleation and growth of ordered regions in specific directions, governed by elastic energy [32]. The twin structures are formed when transformation strains accumulate, as in the disorder-ordered phase transformation in $(Fe_{1-x}Co_x)_{59}Pt_{41}$ films.

In the $(Fe_{1-x}Co_x)_{59}Pt_{41}$ films, the ordering parameter of the ternary alloy is lower than that of $Fe_{59}Pt_{41}$. There is a strong correlation between degree of ordering and

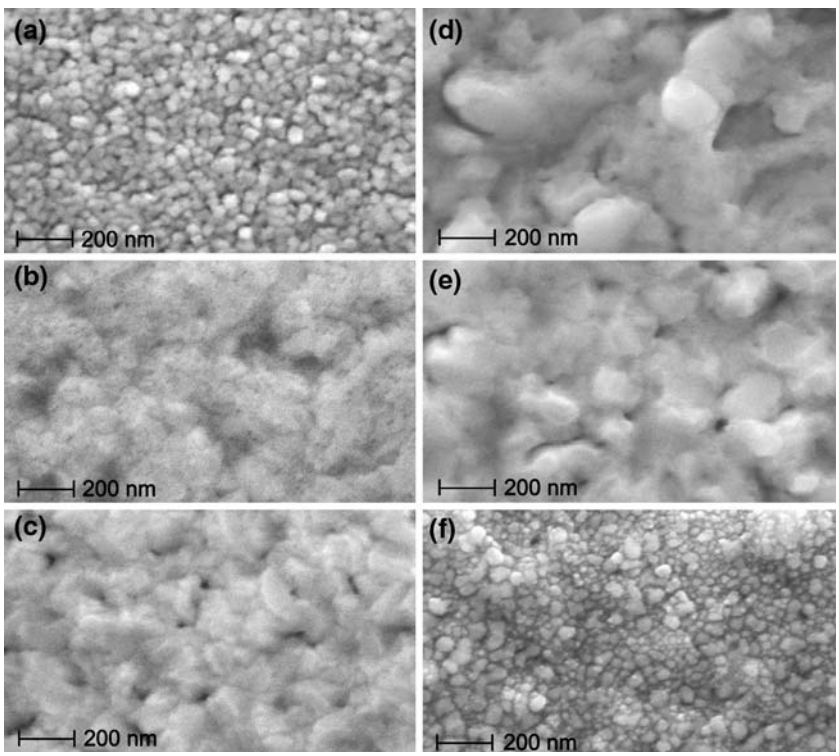

Fig. 4 SEM micrographs of the as-deposited thin films upon the Pt underlayer; (**a**) $Fe_{59}Pt_{41}$; (**b**) $(Fe_{0.8}Co_{0.2})_{59}Pt_{41}$; (**c**) $(Fe_{0.6}Co_{0.4})_{59}Pt_{41}$; (**d**) $(Fe_{0.4}Co_{0.6})_{59}Pt_{41}$; (**e**) $(Fe_{0.2}Co_{0.8})_{59}Pt_{41}$; (**f**) $Co_{59}Pt_{41}$

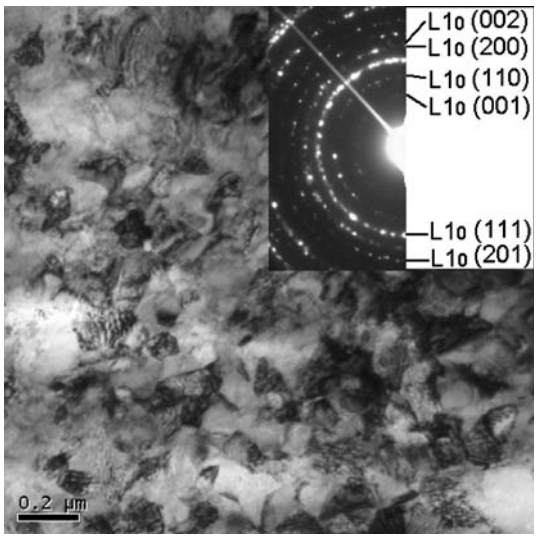

Fig. 5 The bright-field TEM image and electron diffraction pattern of the $(Fe_{0.8}Co_{0.2})_{59}Pt_{41}$ alloy film

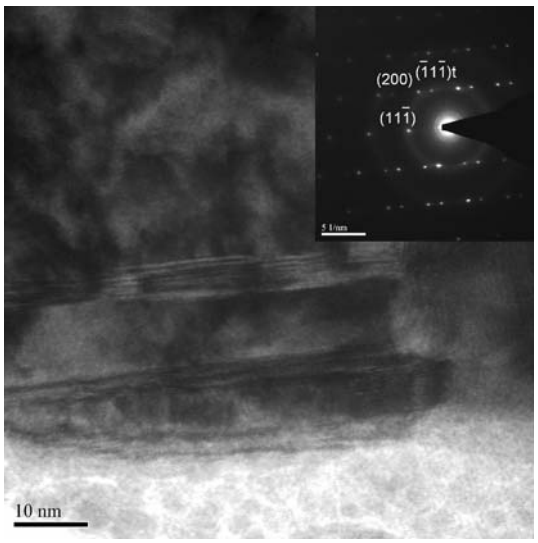

Fig. 6 The TEM images of $(Fe_{0.8}Co_{0.2})_{59}Pt_{41}$ cross-section film. The TEM image shows planar defects of twins. The inset shows the selected area diffraction (SAD) pattern

coercivity. The $Fe_{59}Pt_{41}$ has a coercivity of about 10 kOe, which exceeds that of the ternary alloy, which is around 3 kOe. Figure 7 plots the hysteresis loops measured perpendicular to the $(Fe_{1-x}Co_x)_{59}Pt_{41}$ alloy film plane (substrate). The $Fe_{59}Pt_{41}$ film had a higher coercivity than that of ternary alloy because it had a higher degree of ordering. For the $Co_{59}Pt_{41}$ film, the ordering parameter dropped steeply, indicating that the alloy contained fewer ordered regions, minimizing Hc to around 800 Oe. The twin boundaries present in the $(Fe_{0.8}Co_{0.2})_{59}Pt_{41}$ alloy film may act as pinning sites but the density of twins was not sufficiently high to cause high magnetic hardness. However,

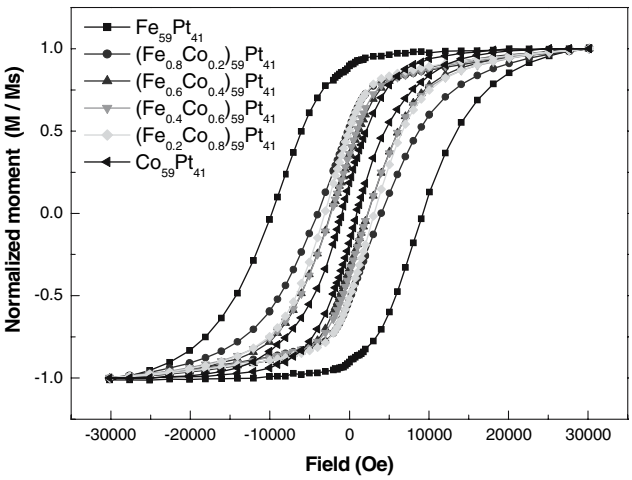

Fig. 7 Hysteresis loops measured in a perpendicular direction of the $(Fe_{1-x}Co_x)_{59}Pt_{41}$ alloy films annealed at 600 °C for 1 h (x = 0, 0.2; 0.4; 0.6; 0.8; 1)

the saturation magnetization, Ms, of the $(Fe_{0.8}Co_{0.2})_{59}Pt_{41}$ film is about 1,480 emu/cm^3 higher than that of $Fe_{59}Pt_{41}$. Forming the FeCo metal bond with an fct structure probably maximizes the Ms of FeCo alloy to approximately 1,600 emu/cm^3, as governed by both the direction of deposited atoms and thermal diffusion of the temperature necessary for deposits [2, 33, 34]. Figure 8 plots other correlations of the magnetic characteristics of the $(Fe_{1-x}Co_x)_{59}Pt_{41}$ films. The Hc = 3,000 Oe of $(Fe_{0.2}Co_{0.8})_{59}Pt_{41}$ exceeds Hc = 2,500 Oe for $(Fe_{0.4}Co_{0.6})_{59}Pt_{41}$. For ternary alloy films, the degree of ordering in $(Fe_{0.2}Co_{0.8})_{59}Pt_{41}$ was similar to others, suggesting that the slight increase in Hc may have been caused by defects in the single grain that serve as pinning sites that impede the motion of the domain walls. A small increase in the amount of 12 at.% Co (x = 0.2) in $Fe_{59}Pt_{41}$, or 12 at.% Fe (x = 0.8)

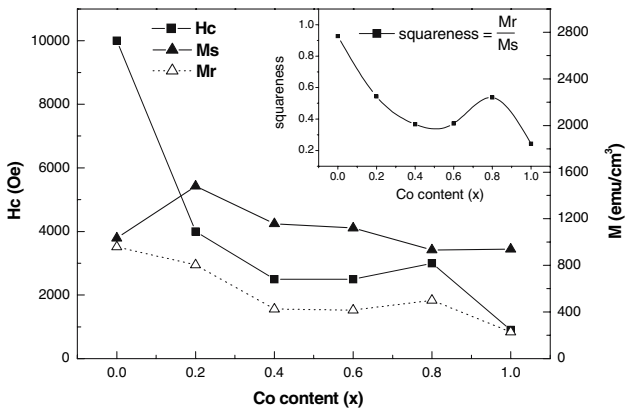

Fig. 8 The dependence of remanence, saturation magnetization, and coercivity measured in the perpendicular directions of $(Fe_{1-x}Co_x)_{59}Pt_{41}$ alloy films on Co concentration (x). The inset shows the variation of squareness as a function of Co concentration

in $Co_{59}Pt_{41}$ can introduce a lattice distortion, which enhanced the coercivity of $(Fe_{1-x}Co_x)_{59}Pt_{41}$ ternary alloy films. The results agree with the first principle calculation by MacLaren et al. [35] in which abnormal anisotropy occurs at around 10 at.% Co doping in FePt alloys, or 10 at.% Fe in CoPt alloys.

The $Fe_{59}Pt_{41}$ has a remnant magnetization (Mr) of about 958 emu/cm^3, which exceeds the Mr of the ternary alloys. The remnant magnetization is the retained amount of irreversible magnetization. The remnant magnetization of $(Fe_{1-x}Co_x)_{59}Pt_{41}$ thin films decreased as the Co content increased. For the $Co_{59}Pt_{41}$ film, the ordering parameter dropped steeply, indicating that it tends to have disordered magnetic properties, minimizing Mr to around 230 emu/cm^3.

For thin films, an out of plane (substrate) applied field inducts a strong demagnetizing field due to the shape effect. The demagnetization has a tendency to align the magnetic moment in the in-plane direction. When alloy films have hard magnetic properties (high Hc), the magnetic moments would be affected insignificantly by the demagnetizing field. Conversely, when the films have soft magnetic properties, the magnetic moments would clearly be affected by the demagnetizing field.

The inset in Fig. 8 plots squareness as a function of Co concentration. The squareness of the ternary alloy, $(Fe_{0.6}Co_{0.4})_{59}Pt_{41}$ had a minimum value of approximately 0.4, because of the demagnetizing field and the varied directions of the *c*-axes in polycrystalline material. On the other hand, Fig. 8 shows that the coercivity of $(Fe_{0.2}Co_{0.8})_{59}Pt_{41}$ was slightly increased. This indicates that alloy film ($x = 0.8$) has a high Hc value. When the alloy film has hard magnetic properties, the magnetic moments would be affected insignificantly by the demagnetizing field. For this reason, the squareness of $(Fe_{0.2}Co_{0.8})_{59}Pt_{41}$ is higher than that of $(Fe_{0.6}Co_{0.4})_{59}Pt_{41}$. Therefore, the trend of squareness of the $(Fe_{1-x}Co_x)_{59}Pt_{41}$ alloy films as a function of Co concentration is similar to the trend of coercivity of the alloy films.

Conclusions

Magnetic $(Fe_{1-x}Co_x)_{59}Pt_{41}$ ($x = 0$, 0.2, 0.4, 0.6, 0.8, 1) alloy films were deposited by DC sputtering on a Si substrate with a Pt film as an underlayer. At $T_s = 500$ °C, the surface morphology of ternary alloy films changed due to alloying with the third element, Co. The $L1_0$ phase of iron-rich alloy films begins to appear when the sample is deposited at $T_s = 500$ °C. Following annealing, the binary $Fe_{59}Pt_{41}$ film has high coercivity of about 10 kOe because of its high degree of ordering. The temperature required for the formation of the $L1_0$ phase increases according to the number of Co atoms replacing Fe atoms, and the coercivity and squareness decline as the Co content increases. The saturation magnetization correlation with the switching field is important for recording performance as well as the coercivity for stability in maintaining data. The amount of saturation magnetization was determined by the intrinsic composition of alloy film. In the $(Fe_{1-x}Co_x)_{59}Pt_{41}$ alloy films, the composition $(Fe_{0.8}Co_{0.2})_{59}Pt_{41}$ has the highest saturation magnetization. The saturation magnetization of the $(Fe_{0.8}Co_{0.2})_{59}Pt_{41}$ alloy film is improved to about 1,480 emu/cm^3 higher than 1,140 emu/cm^3 for FePt [11] and 800 emu/cm^3 for CoPt [2], respectively. Furthermore, in contrast with FePt, the transition from the disordered fcc phase to the $L1_0$ phase in the $(Fe_{0.8}Co_{0.2})_{59}Pt_{41}$ film is only slightly influenced by Co addition, where the Fe atoms were fully replaced with Co atoms, the required ordering temperature for CoPt is too high to utilize in the practical applications.

Acknowledgments The authors would like to thank the National Science Council of the Republic of China for the financial support of project NSC 95-2221-E-006-121.

References

1. Bozorth RM (1993) Ferromagnetism. New York IEEE Press, p33
2. Burkert T, Nordstrom L, Eriksson O, Heinonen O (2004) Phys Rev Lett 93:027203
3. Ostanin S, Razee SSA, Staunton JB, Ginatempo B, Bruno E (2003) J Appl Phys 93:453
4. Zhang Y, Wan J, Bonder MJ, Hadjipanayis GC, Weller D (2003) J Appl Phys 93:7175
5. Visokay MR, Sinclair R (1995) Appl Phys Lett 66:1692
6. Sakuma A (1994) J Phys Soc Jpn 63:3053
7. Huang YH, Okumura H, Hadjipanayis GC (2002) J Appl Phys 91:6869
8. Kronmuller H, Fahnle M (2003) Micromagnetism and the microstructure of ferromagnetic solids. Cambridge University Press, Cambridge, p90
9. Liu JP, Lio CP, Liu Y, Sellmyer DJ (1998) Appl PhysLett 72:483
10. Shima T, Takanashi K (2004) Appl Phys Lett 85:2571
11. Weller D, Moser A, Folks L, Best ME, Lee W, Toney MF, Schweickert M, Thiele JL, Doerner MF (2000) IEEE Trans Magn 36:10
12. Seki T, Shima T, Takanashi K, Takahashi Y, Matsubara E, Hono K (2003) Appl Phys Lett 82:2461
13. Mitani S, Takanashi K, Sano M, Fujimori H, Osawa A, Nakajima H (1995) J Magn Magn Mater 148:163
14. Chen SC, Kuo PC, Kuo ST, Sun AC, Lie CT, Chou CY (2003) Mat Sci Eng B 98:244
15. Chen M, Nikles DE (2002) Nano Lett 2:211
16. Sato T, Goto T, Ogata H, Yamaguchi K, Yoshida H (2002) J Magn Magn Mater 272–276:e951
17. Saha S, Thong CJ, Huang MQ, Obermyer RT, Zande BJ, Chandhok VK, Simizu S, Sankar SG (2002) J Appl Phys 91:8810
18. Kanazawa H, Lauhoff G, Suzuki T (2002) J Appl Phys 87:6143
19. Watanabe K, Masumoto H (1983) Mater Trans JIM 24:627
20. McHenry ME, Laughlin DE (2000) Acta Mater 48:223

21. Singleton EW, Narayan PB, Xiong W, Raman R, Hoo HL (1999) J Appl Phys 85:5840
22. Donald L Smith (1994) Thin-film deposition principles and practice. McGraw-Hill, p 592
23. Takahashi YK, Ohnuma M, Hono K (2002) J Magn Magn Mater 246:259
24. Cebollada A, Weller D, Sticht J, Harp GH, Farrow RFC, Mark RF, Savoy R, Scott JC (1994) Phys Rev B 50:3419
25. Cullity BD (1978) Elements of X-ray diffraction. Addison-Wesley 2st edn, p 520
26. Barmak K, Kim J, Shell S, Svedberg EB (2002) Appl Phys Lett 22:4268
27. Massalski TB (1986) Binary alloy phase diagrams. Metallurgical Society of AIME 1, p1096 and p791
28. Zhao ZL, Ding J, Inaba K, Chen JS, Wang JP (2003) Appl Phys Lett 83:2196
29. Toney MF, Lee WY, Hedstrom JA, Kellock A (2003) J Appl Phys 93:9902
30. Pynko VG, Komalov AS, Ivaeva LV (1981) Phys Stat Sol 63a:127
31. Hong MH, Hono K, Watanabe M (1998) J Appl Phys 84:4403
32. Zhang B, Lelovic M, Soffa WA (1991) Script Met Mat 25:1577
33. Chang WC, Lin CC, Chang HW, Chiu CH, Chen SK (2006) Surf Coat Technol 200:3366
34. Suzuki Y, Haimovich J, Egami T (1987) Phys Rev B 35:2162
35. MacLaren JM, Willoughby SD, McHenry ME, Ramalingam B, Sankar SG (2001) IEEE Trans Magn 37:1277